Published in final edited form as:
J Am Chem Soc. 2013 June 26; 135(25): 9465–9474. doi:10.1021/ja404305k.

The Role of Ligands on the Equilibria Between Functional States of a G Protein-Coupled Receptor

Tae Hun Kim[a], **Ka Young Chung**[b,c], **Aashish Manglik**[b], **Alexandar L. Hansen**[d], **Ron O. Dror**[e], **Thomas J. Mildorf**[e], **David E. Shaw**[e,f], **Brian K. Kobilka**[b], and **R. Scott Prosser**[a,*]

[a]Department of Chemistry, University of Toronto, UTM, 3359 Mississauga Rd. N, Mississauga, ON, Ontario L5L 1C6, Canada

[b]Department of Molecular and Cellular Physiology, Stanford University School of Medicine, Stanford, California, 94305

[c]School of Pharmacy, Sungkyunkwan University, Suwon 440-746 South Korea

[d]Department of Medical Genetics and Microbiology, University of Toronto, Toronto, ON, Ontario M5S 1A8, Canada

[e]D. E. Shaw Research, New York, New York 10036, USA

[f]Center for Computational Biology and Bioinformatics, Columbia University, New York, New York 10032, USA

Abstract

G protein-coupled receptors (GPCRs) exhibit a wide variety of signaling behaviors in response to different ligands. Using a small label on the cytosolic interface of TM6 (Cys-265), ^{19}F NMR spectra of the β_2 adrenoreceptor, β_2AR, reconstituted in maltose–neopentyl glycol detergent micelles, revealed two distinct inactive states, an activation intermediate state en route to activation, and, in the presence of a G protein mimic, a predominant active state. An analysis of spectra as a function of temperature reveals that for all ligands, the activation intermediate is entropically favored and enthalpically disfavored. β_2AR enthalpy changes toward activation are notably lower than those observed with rhodopsin – a likely consequence of basal activity and the fact that the ionic lock and other interactions stabilizing the inactive state of β_2AR, are weaker. Positive entropy changes toward activation likely reflect greater mobility (configurational entropy) in the cytoplasmic domain, confirmed through an order parameter analysis. Ligands greatly influence overall changes in enthalpy and entropy of the system and corresponding changes in population and amplitude of motion of given states, suggesting a complex landscape of states and substates.

*To whom correspondence should be addressed. R. Scott Prosser Department of Chemistry, University of Toronto, UTM, 3359 Mississauga Rd. N, Mississauga, ON, Ontario L5L 1C6, Canada 905-828-3802 scott.prosser@utoronto.ca.

SUPPORTING INFORMATION

Figures S1. Deconvolutions of ^{19}F NMR spectra of β_2AR, as a function of ligand. S2. Deconvolutions as in S1, assuming a single inactive state. S3. Characteristic T_2 relaxation series, showing deconvolutions and typical noise. S4. (as in S3, assuming a single inactive state. S5. Comparison of spectra as a function of signal to noise ratios. S6. Relative population of states as a function of ligand. S7. Orientational order parameters and correlation times as a function of ligand. S8. van't Hoff analysis of populations. S9. ^{19}F NMR study after protease digestion. Table T1. Comparison of rates extracted from deconvolutions and from T_2 relaxation experiments. Table T2. Complete analysis of relaxation rates, order parameters and correlation times as a function of ligand. This material is available free of charge via the Internet at http://pubs.acs.org.

Keywords

β2 adrenoreceptor; ^{19}F NMR; GPCR dynamics

INTRODUCTION

In eukaryotes, signal transduction across the cell membrane is routinely achieved through G protein-coupled receptors (GPCRs), which respond to light or a variety of ligands including hormones, lipids, and neurotransmitters[1–5]. Their activation, by either light or binding ligand, then initiates an interaction with a specific intracellular guanine nucleotide binding protein (G protein), leading to release and activation of the alpha subunit and downstream activation of specific signaling pathways. While most GPCRs have a similar topology, consisting of seven transmembrane alpha helical segments, separated by intra- and extracellular loops[6], there is an enormous variation in ligand-dependent signaling behavior among the nearly 800 human GPCRs.

The classic view of the mechanism of action of GPCRs is that ligand binding to the extracellular pocket induces a local perturbation, which triggers a conformational change on the intracellular side associated with the G protein binding interface. Computational and experimental studies suggest that this picture is over simplified and that, in the case of ligand-activated GPCRs, the active state is thermally accessible, though generally weakly populated without the addition of agonist[7,8]. Computational studies describe the GPCR in terms of a loosely coupled allosteric network in which distinct regions of the protein may switch between conformations consistent with inactive and active states[9]. Ligands play a key role in stabilizing or destabilizing intermediates involved in activation. For example, upon binding to an agonist, a GPCR con-former is then stabilized for a sufficient period of time to engage a G protein[10]. This picture is reminiscent of the recent NMR-based perspective, which purports that many enzymes are inherently plastic and conformations associated with activation intermediates are frequently sampled. In this case, the role of the substrate is to alter the stability of key on-pathway intermediates[11]. While the entirety of ligand-dependent activation pathways is admittedly complex, it is insightful to identify key activation intermediates and the associated changes in amplitudes and timescales of domain-specific motions, upon addition of ligand. Alternatively, a thermodynamic approach may be taken in an attempt to understand the role of ligands in activation. For example, a positive enthalpy change upon activation often reflects the loss of stabilizing interactions associated with the inactive state, while entropy gains can be associated with increased protein dynamics or the release of waters of hydration.

In this work on the human β_2 adrenoreceptor, β_2AR, we employ ^{19}F NMR to examine the functional states associated with the GPCR, reconstituted in maltose–neopentyl glycol (MNG-3) detergent micelles. By quantifying the relative fraction of each of the states as a function of temperature, we are able to map out the thermodynamic equilibria between inactive states, an activation intermediate state, and active states. A van't Hoff analysis of these equilibria provides enthalpy and entropy differences between states, which can be further evaluated in the presence of various ligands and a nanobody (Nb80) G protein mimic[12,13]. Finally, an analysis of ^{19}F NMR spin relaxation rates, provides a molecular perspective of both the amplitude and timescale associated with local motions in the cytoplasmic domain, known to interact with the G protein[14,15]. We discuss these results in terms of our current understanding of the mechanism of action of GPCRs and the role of ligands in the process.

RESULTS

In the absence of G protein or a G protein mimic, ^{19}F NMR spectra associated with Cys-265 may be attributed to three states. To delineate functionally distinct states we have employed a trifluoromethyl tag (–$COCF_3$) located on Cys-265, near the cytosolic water interface of TM6. Crystal structures of the inactive and active forms of β_2AR reveal that TM6 is displaced outward from the helical bundle upon activation, such that Cys-265 becomes more solvent exposed in the active state[16]. Since ^{19}F NMR chemical shifts are sensitive to electrostatic environments and van der Waals contacts[17], Cys-265 is an ideal labeling site to distinguish conformers related to activation. Indeed, Cys-265 has been used previously in fluorescence spectroscopy[18] and ^{19}F NMR studies[19,20] to monitor receptor activation[21]. The ^{19}F NMR spectrum of the apo form of β_2AR is shown in Figure 1. This spectrum can be deconvolved into three components, designated S_1, S_2, and S_3, which we attribute to Cys-265, and a fourth component, designated as **A**, arising from an additional cysteine residue. We note that all spectra presented in this paper (See Supplementary Figure S1), were obtained from β_2AR, reconstituted in maltose–neopentyl glycol (MNG-3) detergent micelles, which in our hands gives rise to greater chemical shift dispersion and greater sample stability than that in DDM[20].

An alternative deconvolution of the apo β_2AR spectrum into two states, $S_{1,2}$ and S_3, is provided in Supplementary Figure S2, where the residual error in the fit is noted to be greater than the noise. Our choice of assigning three states to the protein, is partly based on the observation that the fitted line widths of S_1, S_2, and S_3 correspond well to the line widths estimated from T_2 relaxation measurements. In contrast, the line width of $S_{1,2}$ resulting from the assumption of two states, is significantly greater than that estimated by T_2 measurements, suggesting $S_{1,2}$ is best represented by two or more peaks, as discussed at length in Supplementary Figure S3 and S4 and Supplementary Table T1. Based on T_2 measurements, which essentially permit us to evaluate the line widths of states, independent of the deconvolution, this assumption of three states holds true for all ligands investigated.

The relative population of the three states depends on ligand

Remarkably, the addition of saturating amounts of inverse agonist (carazolol, denoted Cz), partial agonist (salmeterol, denoted Salm), or agonist (BI-167107, denoted as BI), results in spectra, all of which may be characterized by the same three states, as defined in Figure 1. These spectra and their deconvolutions are shown in a recently published article[20] and in Supplementary Figure S1. The principle effect of the ligand is to alter populations of states S_1, S_2, and S_3. The absence of gross differences in line width or frequency suggests that the states, S_1, S_2, and S_3 are in slow exchange on an NMR time scale (*i.e.* < 150 s^{-1}). However, given the small differences in chemical shifts between states[22–24], it is difficult to study details of exchange dynamics via saturation-transfer or CPMG relaxation experiments, which ideally rely upon a sizeable chemical shift difference between states. Note that a second weak peak, denoted as Δ, appears in all spectra near −84.15 ppm. The integral associated with this peak is unchanged by ligand, and thus likely arises from another labeled cysteine residue that is not sensitive to conformational changes (*vide infra*).

Spectral deconvolutions such as those provided above, require high fidelity spectra with very good *signal to noise* (S/N) ratios. This is further explained in Figure 2, where ^{19}F NMR spectra of inverse agonist and nanobody-stabilized GPCR are shown in Figure 2a and 2c, respectively. Upon identifying the best-fit frequencies and widths of states S_1, S_2, and S_3 in Figure 2a, a range of offset frequencies are applied to the peak associated with state S_1, whereupon a global deconvolution is attempted, allowing all other parameters to vary. The resulting root mean square deviation (RMSD) for each fit is then normalized by dividing by the RMSD obtained for the greatest chemical shift offset for S_1. This exercise is then

repeated for states S_2, and S_3, as shown in Figure 2b (See green, blue, and red triangles). The results show that the RMSD fitting error in the global deconvolution more than doubles when an offset of ±0.04 ppm is attempted for any peak, suggesting that all three states, S_1, S_2, and S_3 are robustly defined. Note that the addition of noise to these spectra quickly changes the outcome, as shown in Figure 2b and Supplementary Figure S5. When the S/N ratio is reduced by more than a factor of two, the deep fitting minima disappear and it is difficult to define three distinct frequencies, and hence, three distinct states. Figure 2d shows a similar analysis for the ^{19}F NMR spectrum of β_2AR, stabilized by BI agonist plus the G protein mimic, Nb80. In this case, the RMSD error resulting from offsetting either S4a, S4b, or S4c, does not change as precipitously as that shown in Figure 2b. We conclude that the nanobody spectrum is characterized by a prominent single (fully active) state, S_{4a}, with the possibility of additional minor conformers, characterized by more downfield shifts.

The results of the spectral deconvolutions as a function of ligand and nanobody are shown in Figure 3 (and Supplementary Figure S6), where the relative populations of S_1, S_2, and S_3 are expressed as a function of ligand, using the areas of deconvolved peaks. Based upon the effects of inverse agonist and agonist on the relative populations of S_1, S_2, and S_3, we assign S_1 and S_2 to distinct inactive state conformers and S_3 to an intermediate associated with activation of β_2AR. Note that the addition of agonist increases the fraction of the S_3 state, which also appears most upfield. The active conformation of β_2AR is characterized by an outward shift of the intracellular end of TM6, which is consistent with the more upfield chemical shift of the activation intermediate, S_3, since greater solvent exposure typically results in upfield ^{19}F NMR chemical shifts[17]. Clearly, the nanobody has the effect of stabilizing a single (active) state, with the possibility of two minor conformers as discussed above.

The functional states can be described in terms of local orientational order and dynamics

While the spectral deconvolutions and T_2-based line width analyses confirm the existence of distinct inactive, intermediate, and fully active states associated with the G protein binding domain, we can further delineate these states in terms of local reorientational dynamics. We begin by assuming the dynamics of the fluorinated reporter can be described in terms of a tumbling time, τ_M, associated with the detergent solubilized GPCR, and a correlation time, τ_e, associated with the much faster reorientations of the trifluoromethyl group at the cytosolic interface. τ_M can be estimated from experimental measures of the hydrodynamic radius, r_H, of the detergent solubilized GPCR, which is in turn derived from diffusion rate measurements, which monitor the aromatic (protein) signal as a function of gradient strength in a pulsed field gradient stimulated echo diffusion experiment[25]. The amplitude associated with these fast local reorientations, is described by an orientational order parameter, S^2, where S^2=0 is equated with unrestricted local reorientations and S^2=1 is associated with a completely rigid probe. S^2 and τ_e can then be reliably ascertained by a model-free analysis of ^{19}F NMR relaxation times, T_1, and T_2, at two field strengths (in our case, 600 MHz and 500 MHz ^{1}H Larmor frequencies, data shown in Supplementary Table T2)[14,15].

The model-free analysis yielded a clear trend with regard to orientational amplitudes associated with the probes in each of the three states, S_1, S_2, and S_3, as shown in Figure 4. In all cases, the orientational order is lowest for the activation intermediate. At the same time, the timescale, τ_e, is generally largest for the activation intermediate, as shown in Figure 4 and Supplementary Figure S7. The dominant active state, S_{4a} exhibits comparable flexibility with the activation intermediate, S_3. We note that our trifluoromethyl $COCF_3$ probe may exhibit residual mobility that is different from seen with CH_2CF_3[19] tags and indeed other trifluoromethyl tags[26]. For this reason, we rely on S^2 to describe relative mobility of distinct states as a function of ligand.

For all ligands considered, activation is entropically driven and enthalpically disfavored

To further explore the role of specific states in GPCR activation, we have conducted a careful analysis of the ^{19}F NMR spectra as a function of temperature. Using the deconvolved spectra, it is possible to interpret the ratio of areas, associated with S_1, S_2, and S_3 in terms of equilibrium constants, K_{12}, K_{23}, and K_{13} (data shown in Supplementary Figure S8). Assuming the state-specific enthalpies are constant over the temperature range investigated, the temperature dependence of the equilibria between states *i* and *j* may be expressed by the van't Hoff equation (Equation 1),

$$\ln K_{ij} = \frac{\Delta\Delta H_{ij}}{RT} + \frac{\Delta S_{ij}}{R} \quad (1)$$

where ΔH_{ij} and ΔS_{ij} represent the enthalpy and entropy differences between states, R is the gas constant, and T represents the temperature. Figure 5a shows a van't Hoff analysis for the agonist-saturated β_2AR sample. The results of this analysis are shown in Figure 5b and 5c, where relative differences in enthalpy, ΔH_{ij}, and entropy, ΔS_{ij}, are given. Note that in some cases it was only possible to reliably discriminate two states over the entire temperature range. In these cases, the equilibria and corresponding thermodynamic parameters differentiate a state representing an average of the two inactive states, from the activation intermediate; the equilibria are thus reported as $K_{(1,2),3}$ or $K_{(4b,4c),4a}$.

DISCUSSION

States and Populations

A significant body of evidence suggests that GPCRs are not simple two-state switches but rather encompass a wide spectrum of states and conformations[5,27,28]. Recent spectroscopic studies have echoed the suggestion of multiple states[20,28,29]. For example, Liu *et al* examined the idea of biased agonism, showing evidence for specific ligands favoring one of two conformations, thereby selecting for distinct signaling pathways[19]. In the current study, two inactive states, S_1 and S_2, account for roughly 60% of the total spectral intensity for the apo and inverse agonist saturated samples. Recent MD simulations of the inactive state of β_2AR reveal an alternative inactive conformer, in which the intracellular half of TM7 (Asn318-Cys327, including the conserved NPxxY motif) is rotated ~40° clockwise relative to the crystal structure (viewed from the intracellular side) and shifted toward the center of the helical bundle by ~3 Å[9,29]. This state is believed to exchange slowly with the crystallographically observed inactive state in the presence of inverse agonists or in the absence of a ligand[29]. Thus, it seems likely that S_1 and S_2 represent two distinct inactive state conformers. Interestingly, the effect of partial agonist, salmeterol, seems to favor the S1 state, as shown in Figure 2. The addition of agonist similarly favors S_1 over S_2 though by far the greatest effect of agonist is to stabilize the S_3 state.

A recent NMR study of β_2AR also identified two distinct inactive states and an agonist activated state[28]. Here, both inactive states are comparably populated upon addition of inverse agonist (Cz), while the addition of agonist causes an increase in the population of S_3, which we assign to an activation intermediate. We note that the observation of three distinct states was only possible with the new detergent, MNG-3[20]. How exactly these three states relate to the observation of two states and the concept of biased agonism is unclear, since the study by Liu *et al* [19] was performed using DDM micelles, which in our hands gives rise to a degree of motional narrowing, and might therefore mask additional states[20]. It was also only possible for us to delineate three states, after achieving exceptional signal to noise for all spectra, as outlined in Figure 2. Moreover, we can be confident that the states S_1, S_2, and S_3

are distinct and functional since all samples were purified in the final step by ligand affinity chromatography and all states respond to both ligand and the addition of nanobody.

Dror *et al* have utilized molecular dynamics simulations, beginning with a G-protein stabilized active conformation[16], to identify an on-pathway intermediate state of the G protein binding domain[9]. Both the intermediate and active conformations are distinguished by a progressive outward shift of the intracellular end of TM6. These same authors also proposed that the G protein may first bind to the GPCR in the intermediate state. Binding then promotes conversion to the active state. We conclude that S_3 represents an on-pathway intermediate towards a fully active state, which is achieved upon binding to either a G protein or a G protein mimic. This same conclusion was recently reached in an NMR study of ^{13}C-methionine enriched β_2AR[29]. There is also some recent evidence to suggest that rhodopsin exhibits similar behavior in the sense that the light activated state (Rho*) exhibits a different topology from the fully active complex with the G protein (Rho*-G_t), based on radiolytic footprinting and deuterium exchange studies[30].

The addition of a G protein mimetic nanobody (Nb80) is believed to fully stabilize the active conformation of β_2AR[12]. In our hands, the addition of Nb80 resulted in a completely distinct peak, denoted S_{4a} in Figure 2, with two smaller peaks, denoted S_{4b} and S_{4c}. Since Cys-265 is known to be more than 5 Å from the van der Waals surface of Nb80, based on computational analysis, it is more likely that the shift arises from a conformational change to a distinct active state, rather than a chemical shift perturbation due to binding of Nb80 (Note that the A peak does not shift upon addition of Nb80). Binding of the nanobody presumably reinforces the entire structure such that it adopts a fully active state, designated as S_{4a}, while S_{4b} and S_{4c} may represent distinct minor conformers, possibly resulting from alternate modes of interaction between the receptor and the nanobody. β_2AR couples the binding of specific agonists to the activation of either the stimulatory or inhibitory heterotrimeric G proteins, G_s and G_i, while alternatively signaling through MAP kinase pathways in a G-protein-independent manner via β-arrestin[31]. Given the signaling promiscuity of β_2AR, one can well imagine an active state or an activation intermediate, whose conformation is compatible with one or more G proteins and which then adopts the appropriate G protein specific conformation via a combination of presampling and induced fit. The minor states, S_{4b} and S_{4c}, could therefore represent alternative active states that are stabilized by interactions with G_i or β-arrestin mimics, though this remains to be shown. Alternatively, the minor states might be necessary for facilitating the process of deactivation or G protein decoupling. While outside the current scope of this paper, it is feasible that the active state ensemble may indeed consist of a number of stable conformations.

Clearly, ligands predominantly influence the populations of a distinct ensemble of states, though there may well be an accompanying change in lifetime of these states. It is however, surprising that the addition of inverse agonist and partial agonist causes a relatively small change in populations of states. A recent NMR study examined spectra from ^{13}C-methionine enriched β_2AR, where the authors identified key regions of the transmembrane domains in which two distinct inactive states could also be observed[28,29]. While their observations are similar to ours, the relative populations are quite different, and the activation intermediate is only apparent upon addition of agonist. Part of this apparent difference arises from the fact that the relative volume of a peak in a two dimensional ^{13}C,^{1}H spectrum is not representative of the population, since the requisite INEPT transfer periods cause significant losses in intensity of the peaks with the lowest T_2 relaxation times. In ^{19}F NMR, or indeed any directly detected one-dimensional NMR technique, the relative areas of deconvolved peaks should faithfully reproduce the relative populations. A weak response to ligand through populations, assessed from a single domain, may be a consequence of the fact that the GPCR is a loosely coupled system. Distinct changes in the ligand binding domain give

rise to probabilistic changes in the conformers associated with the connecting region and cytosolic domain of the GPCR. However, the changes in lifetimes and dynamics of states, with ligand, may play a key role in affecting activation. Alternatively, the weak response to ligands measured here may reflect the fact that our measurements are sensitive only to a subset of the degrees of freedom of the G protein binding domain.

Order and Dynamics

The motional amplitudes of distinct states are also greatly influenced by the ligand, as depicted in Figure 6. Note that the activation intermediate exhibits the greatest amplitude of motion, regardless of ligand. Molecular dynamics (MD) simulations and crystallography studies of agonist saturated β_2AR tend to result in a single low-energy state consistent with the inactive conformation so it is perhaps not surprising that the activation intermediate state exhibits the largest amplitude, fast-timescale (sub nanosecond) dynamics, at least prior to binding to the G protein mimic. Higher disorder of the G-protein binding region would also provide greater conformational plasticity needed to achieve efficient coupling to the G protein, if the interaction is facilitated by an induced fit mechanism[32].

Figure 6 also illustrates the idea that orientational order is also greatly influenced by ligand. Note in particular that the addition of agonist results in overall greater rigidity of states S_1 and S_2 from that observed with inverse agonist, while the orientational order of the activation intermediate is unchanged with ligand. One can interpret the orientational order in terms of averaging of underlying fast-timescale substates; a higher order parameter represents a more restricted ensemble of sub-states[10]. Agonist both increases the relative population of the activation intermediate, while at the same time restricting the ensemble of substates for S_1 and S_2. Inverse agonist has exactly the opposite effect - *i.e.* greater disorder among the inactive states and a wider spectrum of substates within S_1 and S_2, while S_3 remains the most dynamic of all states for all cases. Thus, while ligands clearly influence populations of states, there is a pronounced effect of ligand on the average orientational order of states, and in particular, the inactive states. One interpretation is that a given state represents an average over rapidly interconverting substates, whose distribution and inter-conversion rates define the roughness of the landscape. Ligands, influence the substate distribution and roughness, which presumably affects the overall lifetimes and exchange rates of states. For example, addition of agonist causes the reorientational amplitude of the S_1 state to decrease while that of S_2 increases, in comparison to the apo state, which presumably influences activation kinetics and pathways.

Thermodynamics of activation

As shown in Figure 5, an analysis of the temperature dependence of the populations of states, S_1, S_2, and S_3, reveals that activation is enthalpically unfavorable and entropically favorable, regardless of the ligand. We emphasize that these results pertain to the system (GPCR plus water) as a whole, despite the fact that the spectroscopic reporter is confined to a single residue on the protein. The enthalpy and entropy differences associated with activation from rhodopsin to a Meta I intermediate and from the Meta I intermediate to the Meta II active state are also shown in Figure 5, based upon values reported in the literature[5,33]. While rhodopsin activation is also enthalpically unfavorable and entropically favorable, the magnitude of the activation steps are smaller in the case of β_2AR, for any ligand investigated. The differences in enthalpy likely relate to the fact that β_2AR exhibits basal activity whereas rhodopsin requires strict control; the active state is only attained once retinal has undergone a light induced cis-trans isomerization[34,35]. The rhodopsin inactive state is partly stabilized through a socalled ionic lock, which holds together helices 3 and 6 and serves as a molecular switch[18,34,35]. In other words, the rhodopsin inactive state is considerably more stable and requires a greater net input of energy to activate. In contrast,

recent MD simulations and X-ray crystallographic studies of β_2AR reveal that the inactive state exists in equilibrium between a state in which the ionic lock is engaged and one where it is released[36,37]. Thus, net enthalpy changes towards activation are smaller for β_2AR than those observed for rhodopsin. As shown in Figure 5, there is a very clear trend with regard to the enthalpy change toward activation of β_2AR as a function of ligand. Enthalpy changes toward activation are greatest for Cz-bound β_2AR, likely reflecting the additional stability conferred to the inactive state in the vicinity of the binding pocket. In the agonist bound state, enthalpy changes are smallest, reflecting the underlying destabilizing effect of the agonist on the inactive state. Finally, the partial agonist, salmeterol, also exerts a dramatic influence on the enthalpy differences between states, S_1, S_2, and S_3, although activation to S_3 is clearly enthalpically unfavorable and entropically favored.

Despite the close similarity between spectra of apo β_2AR and inverse agonist-bound β_2AR (Figure 2), there is a striking difference between the observed enthalpy and entropy changes upon activation. Unliganded β_2AR, which is known to exhibit significant basal activity, exhibits markedly lower enthalpy and entropy differences between the inactive and active intermediate states, S_1, S_2, and S_3 (than inverse agonist-bound β_2AR). This is consistent with the picture emerging from recent MD simulations based upon fully active and inactive X-ray crystal structures, where the GPCR is described as inherently flexible and loosely coupled[9]. This “loose coupling” implies lower barriers toward activation and a lower enthalpic difference between inactive and active states, relative to a strongly coupled receptor, such as rhodopsin.

For all ligands, the trend toward higher entropy upon activation is also consistent with prior observations of rhodopsin. Essentially, we envisage the β_2AR inactive state as being “stiffer” overall, than the activation intermediate. Thus, conversion to the intermediate will involve an even greater increase in entropy, through increased dynamics. Thus, the change in entropy to the activation intermediate is positive, though progressively smaller in magnitude for inverse agonist, apo, and agonist stabilized β_2AR, respectively, reflecting the relative state of “disorder” of the initial (inactive) state. A number of proteins have been recognized to exhibit lower orientational order and higher configurational entropy associated with the active state ensemble, thereby driving activation[38,39]. If the cytosolic domain exhibits a greater amplitude of motion in the activation intermediate state, this may present a way for the protein to sample the active state more frequently. The model free analysis, discussed earlier, also revealed that for any ligand investigated, the activation intermediate exhibits the lowest order parameter and longest correlation time, τ_e This may be important for coupling to the G protein[10].

An entropy increase associated with activation need not arise entirely from increased dynamics. While the order parameter analysis does indeed reveal the amplitude of motions to be greatest for S_3, the positive entropy change also likely arises from the liberation of water. Recently, a 1.8 Å crystal structure of the adenosine A_{2A} receptor revealed a strongly ordered water network in the inactive state[40]. Others have emphasized the importance of conserved waters in the activation process[30,41,42]. The extension of TM6 upon activation would likely disturb this network, thereby releasing ordered waters at the cytoplasmic interface. This process would also contribute to the overall positive entropy change associated with activation, while facilitating binding to the G protein or other effector molecules.

CONCLUSIONS

β_2AR, like many GPCRs is a remarkably versatile signaling molecule, whose activation is exquisitely sensitive to binding ligand. Using a ($COCF_3$) tag on TM6 in the vicinity of the G

protein binding domain, we find evidence for three states, in the absence of nanobody or G protein. We assign these three states to two distinct inactive states and an activation intermediate. The addition of ligands, including inverse agonist, partial agonist, and full agonist changes the relative population of these states. The fully active state, which we presume to be represented by S_{4a}, is only attainable through the addition of a G protein mimetic. Two other minor peaks result from the addition of nanobody, though their role remains uncertain. It is likely that the S_{4a} state represents that crystallized with Nb80 [12] and is highly similar to the receptor conformation seen in β_2AR-Gs complex crystal structure[16]. As such, S_{4a} likely represents the G protein-coupled conformation of the receptor, and is fully competent to signal. It is difficult to speculate about the signaling output of the activation intermediate, S_3. Because the agonist BI increases the proportion of this conformation, it is likely that the intermediate is a conformation associated with G protein recruitment and subsequent signaling. However, it is not possible to determine whether the conformation of the activation intermediate is capable of binding to G protein and inducing nucleotide exchange.

The amplitude and frequencies of local motions associated with the cytosolic domain were also assessed through T1 and T_2 spin-relaxation experiments. The activation intermediate is observed to exhibit the greatest amplitude of motion, in the apo state or in the presence of any ligand. Ligands have a profound effect on amplitudes and frequencies of motions, as shown in Figure 6. A thorough analysis of the thermal equilibria between these states reveals that activation is enthalpically disfavored and entropically favored, as has been observed in rhodopsin. Even in the presence of inverse agonist, which stabilizes the inactive state, the enthalpy changes are still not as great as those observed in rhodopsin, reinforcing the picture of β_2AR as a much more dynamic GPCR than rhodopsin, at least in the inactive state. Activation is clearly entropically driven. Positive entropy changes with activation are likely a result of greater motional amplitudes, and consequently greater configurational entropy, in the activation intermediate, as evidenced by the order parameter changes in the cytosolic domain. Water too may play a significant role in activation in that water molecules are released into the bulk phase upon activation, thereby contributing to the overall gain in entropy of the system[9].

The magnitude of the enthalpy and entropy changes are generally lower for β_2AR than for those associated with rhodopsin – a likely consequence of basal activity associated with β_2AR. Moreover, while spectra and relative populations of inactive and activation intermediate states are observed to be very similar in the case of apo and inverse agonist bound β_2AR, the magnitude of the enthalpy and entropy changes associated with activation of the apo state are much lower. This is coincident with greater constitutive activity of the apo state and speaks to the notion of protein plasticity. Future experiments focusing on exchange between functional states should prove insightful towards understanding the influence of ligands on energy barriers between states.

EXPERIMENTAL SECTION

β_2AR-Δ4 generation, purification, and labeling with bromotrifluoroacetone

As previously described[43], we utilized a minimal cysteine version of the β_2AR with the following mutations: C77V, C275S, C378A, and C406A. To facilitate purification of the receptor, an M1 Flag affinity sequence was appended to the amino-terminus and six histidines were appended to the car-boxy-terminus. The β_2AR-Δ4 construct was expressed in Sf9 insect cells using baculovirus derived from the pFastBac system (Invitrogen). Insect cell cultures were grown in the presence of 1 μM alprenolol to increase protein yield.

Cell pellets were lysed by osmotic shock, the membrane fraction was isolated by centrifugation, and membranes containing β_2AR-Δ4 were solubilized in a buffer comprised of 20 mM HEPES pH 7.5, 100 mM NaCl, 1 % dodecylmaltoside (DDM), 0.01 % cholesterol hemisuccinate and 1 μM alprenolol. The solubilized fraction of β_2AR-Δ4 was purified by M1 Flag affinity chromatography to yield biochemically pure receptor. To label the receptor, 50 μM tris(2-carboxyethyl)phosphine (TCEP) was first added to reduce any cross-linked receptor followed by 100 μM 3-Bromo-1,1,1-trifluoroacetone (BTFA). The labeling reaction was incubated on ice for 1 hour and quenched with 2 mM cysteine. Further purification of functional, labeled β_2AR-Δ4 receptor was achieved by alprenolol-sepharose chromatography followed by an M1 Flag chromatography step to concentrate the receptor and exchange the detergent from DDM to MNG-3. Detergent exchange was performed over the course of three hours during which the detergent DDM was gradually replaced with 0.01 % MNG-3. To fully remove alprenolol and produce homogeneously unliganded receptor, the M1 Flag resin was washed for one hour in 0.01 % MNG-3 buffer supplemented with the low-affinity, fast kinetics antagonist atenolol at a concentration of 30 μM. This step was followed by a 30 minute wash with 0.01 % MNG-3 buffer containing no ligand to fully displace bound atenolol. Functional β_2AR-Δ4 in MNG-3 micelles was eluted in 0.01 % MNG-3 buffer supplemented with 1 mM EDTA and 0.2 mg/ml Flag peptide. To ensure full labeling of β_2AR-Δ4, a four fold molar excess of BTFA was again added to the receptor and incubated at 4 °C overnight. Excess BTFA was removed by overnight dialysis in a buffer comprised of 20 mM HEPES pH 7.5, 100 mM NaCl, 0.01% MNG-3. All GPCR samples were confirmed to be in a monomeric form[44]. Finally, the sample was concentrated using a 50 kDa molecular weight cut-off spin concentrator (GE Healthcare) to 60 μM. Ligands and nanobody 80 (Nb80) were added at a saturating concentration of 150 μM and incubated with β_2AR for greater than 24 hours before spectra were acquired. Nanobody 80 was expressed in *Escherichia Coli* and purified as described previously[12].

As bromotrifluoroacetone is a relatively small tag, the labeling protocol also resulted in partial labeling of two additional less exposed cysteine residues, as evidenced by the ^{19}F NMR spectra upon digestion with protease K (Supplementary Figure S9). The total area of the two minor peaks in Figure S9 is roughly 30%. Coincidentally, a peak is identified in the β_2AR spectra, labeled A, which does not respond to ligand or nanobody and represents 27% of the total spectral area. Thus, the peak labeled A is presumed to arise from a separate cysteine. A second very minor peak, labeled * in Figure 2c, is believed to arise from another partially labeled residue. The sum of the areas from * and A are observed to be 30% of the total spectral intensity and are found to be independent of ligand and nanobody.

NMR

Most NMR experiments were performed on a 600 MHz Varian Inova spectrometer, using a cryogenic probe capable of ^{19}F NMR. A limited number of relaxation measurements were also performed on a 500 MHz Varian Unity spectrometer, equipped with a ^{19}F room temperature probe. Typical spectra were acquired with 8192 scans and a repetition time of 1 s, with a $\pi/2$ pulse length of 14.5 us and an acquisition time of 0.25 s. Spectra were processed with MestReNova software. FID signals consisting of 14k complex points in the direct dimension were typically linear predicted for the first 2 to 4 points in the FID, then zero filled to 32k points, and apodized with a Lorentzian filter equivalent to 4 Hz broadening.

T_1 was obtained using an inversion recovery sequence, wherein every second scan involved a simple excitation pulse. Through differencing the two, the spectral intensity thus decays exponentially with the interpulse separation, τ. Generally around 8–9 τ values were used to fit each deconvolved peak to an exponential decay, with a time constant, T_1. T_2 was similarly obtained via a CPMG sequence in which the total evolution time was augmented

for a fixed refocusing frequency. Using 8–9 sampling times, the exponential decay in spectral intensity with time could be fitted to determine a relaxation rate, R_2 ($1/T_2$).

Our choice of three states in the deconvolutions is based on the following observations: 1) A deconvolution consisting of two states produces a fit with residual errors which are well above the noise, as shown in Supplementary Figure S2, 2) The addition of a variety of ligands results in spectra which when deconvolved, independently yield the same three resonances and similar line widths, where the principal difference lies in the relative intensities. Overall, it is necessary to employ three states to describe the effect of all ligands examined, and 3) The line widths derived from a deconvolution into three resonances correspond roughly to the measured T_2 relaxation times. The same analysis, using the assumption of two states, results in a gross discrepancy between the line widths, derived from T_2, and the much broader lines, derived from the deconvolution. More importantly, the line width of the downfield peak, $S_{1,2}$, resulting from the assumption of two states, is significantly greater than that estimated by T_2 measurements. This shows that $S_{1,2}$ is best represented by two or more peaks.

An evaluation of error associated with the deconvolutions into three states was performed by first examining, for each peak, the effect of offset on the global fit, as discussed in the text. The robustness of the fit was also considered as noise was folded into the spectra. Noise spectra were recorded on the spectrometer using identical conditions, though without sample. These noise spectra were then added to the experimental spectra to achieve the desired signal to noise ratios. The analysis revealed that high signal to noise ratios were needed to achieve a robust deconvolution into three states for all ligand samples.

In assessing equilibria between states as a function of temperature, several temperature points were repeated to assure that there were no significant hysteresis effects. At the same time, each temperature analysis required roughly 3 days of NMR time, which placed constraints on sample stability. Generally measurements at temperatures of 30°C or more resulted in changes in the spectra after 7–10 days.

T_1 and T_2 data obtained at two fields for most samples, was combined with estimates for τ_M from 1H diffusion measurements, to estimate τ_e and S^2. The fitting uncertainties in the T_1 and T_2 data were used to generate an input set consisting of thousands of possible values, whereupon a Monte Carlo fit was performed to estimate τ_e and S^2. Using Stokes Law, the rotational correlation time, τ_M, hydrodynamic radius, r_H, and viscosity were calculated based on the decay of the ^1H aromatic protein peaks and water peak (as a function of gradient strength) in a stimulated echo NMR experiment. r_H of the ligand only sample was found to be 3.5 nm with corresponding rotational correlation time of 93.9 ns. r_H of the BI +Nb80 sample is 3.7 nm with rotational correlation time of 111 ns.

Supplementary Material

Refer to Web version on PubMed Central for supplementary material.

Acknowledgments

We are also grateful to Professor Oliver P. Ernst (University of Toronto) and Dr. Adrian Bax (NIH) for helpful discussions.

Funding Sources

RSP acknowledges NSERC (grant number 261980) for a research discovery award. BKK acknowledges NIH (grant NH028471) for funding. KYC acknowledges the National Research Foundation of Korea (NRF) funded by the Ministry of Education, Science and Technology (2012R1A1A1039220).

ABBREVIATIONS

GPCR	G protein-coupled receptor
β_2AR	beta-2-adrenergic receptor
DDM	n-dodecyl β-D-maltoside
MNG-3	maltose-neopentyl glycol
Salm	salmeterol
Cz	carazolol
BI	BI-167107
Nb	nano-body
MD	molecular dynamics
FID	free induction decay
INEPT	Insensitive Nuclei Enhanced by Polarization Transfer

REFERENCES

1. Christopoulos A, Kenakin T. Pharmacol. Rev. 2002; 54:323–374. [PubMed: 12037145]
2. Katritch V, Cherezov V, Stevens RC. Trends Pharmacol. Sci. 2012; 33:17–27. [PubMed: 22032986]
3. Reiter E, Ahn S, Shukla AK, Lefkowitz RJ. Annu. Rev. Pharmacol. Toxicol. 2012; 52:179–197. [PubMed: 21942629]
4. Shukla AK, Xiao K, Lefkowitz RJ. Trends Biochem. Sci. 2011; 36:457–469. [PubMed: 21764321]
5. Park PS-H, Lodowski DT, Palczewski K. Annu. Rev. Pharmacol. Toxicol. 2008; 48:107–141. [PubMed: 17848137]
6. Tate CG, Schertler GF. Curr. Opin. Struct. Biol. 2009; 19:386–395. [PubMed: 19682887]
7. Dror RO, Pan AC, Arlow DH, Borhani DW, Maragakis P, Shan Y, Xu H, Shaw DE. Proc. Natl. Acad. Sci. USA. 2011; 108:13118–13123. [PubMed: 21778406]
8. Rosenbaum DM, Zhang C, Lyons JA, Holl R, Aragao D, Arlow DH, Rasmussen SGF, Choi H-J, DeVree BT, Sunahara RK, Chae PS, Gellman SH, Dror RO, Shaw DE, Weis WI, Caffrey M, Gmeiner P, Kobilka BK. Nature. 2011; 469:236–240. [PubMed: 21228876]
9. Dror RO, Arlow DH, Maragakis P, Mildorf TJ, Pan AC, Xu H, Borhani DW, Shaw DE. Proc. Natl. Acad. Sci. U.S.A. 2011; 108:18684–18689. [PubMed: 22031696]
10. Deupi X, Kobilka BK. Physiology. 2010; 25:293–303. [PubMed: 20940434]
11. Eisenmesser EZ, Millet O, Labeikovsky W, Korzhnev DM, Wolf-Watz M, Bosco DA, Skalicky JJ, Kay LE, Kern D. Nature. 2005; 438:117–121. [PubMed: 16267559]
12. Rasmussen SGF, Choi H-J, Fung JJ, Pardon E, Casarosa P, Chae PS, DeVree BT, Rosen-baum DM, Thian FS, Kobilka TS, Schnapp A, Konetzki I, Sunahara RK, Gellman SH, Pautsch A, Steyaert J, Weis WI, Kobilka BK. Nature. 2011; 469:175–180. [PubMed: 21228869]
13. Steyaert J, Kobilka BK. Curr. Opin. Struct. Biol. 2011; 21:567–572. [PubMed: 21782416]
14. Lipari G, Szabo A. J. Am. Chem. Soc. 1982; 104:4546–4559.
15. Lipari G, Szabo A. J. Am. Chem. Soc. 1982; 104:4559–4570.
16. Rasmussen SGF, DeVree BT, Zou Y, Kruse AC, Chung KY, Kobilka TS, Thian FS, Chae PS, Pardon E, Calinski D, Mathiesen JM, Shah STA, Lyons JA, Caffrey M, Gellman SH, Steyaert J, Skiniotis G, Weis WI, Sunahara RK, Kobilka BK. Nature. 2011; 477:549–555. [PubMed: 21772288]
17. Sykes BD, Weingarten HI, Schlesinger MJ. Proc. Natl. Acad. Sci. USA. 1974; 71:469–473. [PubMed: 4592693]
18. Yao X, Parnot C, Deupi X, Ratnala VRP, Swaminath G, Farrens D, Kobilka B. Nat. Chem. Biol. 2006; 2:417–422. [PubMed: 16799554]

19. Liu JJ, Horst R, Katritch V, Stevens RC, Wüthrich K. Science. 2012; 335:1106–1110. [PubMed: 22267580]
20. Chung KY, Kim TH, Manglik A, Alvares R, Kobilka BK, Prosser RS. J. Biol. Chem. 2012; 287:36305–36311. [PubMed: 22893704]
21. Yao XJ, Velez-Ruiz G, Whorton MR, Rasmus-sen SGF, DeVree BT, Deupi X, Sunahara RK, Kobilka B. Proc. Natl. Acad. Sci. USA. 2009; 106:9501–9506. [PubMed: 19470481]
22. Palmer AG III. Chem. Rev. 2004; 104:3623–3640. [PubMed: 15303831]
23. Kay LE. J. Magn. Reson. 2005; 173:193–207. [PubMed: 15780912]
24. Cavanagh, J.; Fairbrother, WJ.; Arthur, G.; Palmer, I.; Skelton, NJ.; Rance, M. Protein NMR Spectroscopy. Amsterdam: Academic Press; 2010.
25. Tanner JE. J. Chem. Phys. 1970; 52:2523.
26. Kitevski-LeBlanc JL, Prosser RS. Prog. Nucl. Magn. Reson. Spectrosc. 2012; 62:1–33. [PubMed: 22364614]
27. Ghanouni P, Gryczynski Z, Steenhuis JJ, Lee TW, Farrens DL, Lakowicz JR, Kobilka BK. J. Biol. Chem. 2001; 276:24433–24436. [PubMed: 11320077]
28. Kofuku Y, Ueda T, Okude J, Shiraishi Y, Kondo K, Maeda M, Tsujishita H, Shimada I. Nat. Comms. 2012; 3:1045.
29. Nygaard R, Zou Y, Dror RO, Mildorf TJ, Ar-low DH, Manglik A, Pan AC, Liu CW, Fung JJ, Bokoch MP, Thian FS, Kobilka TS, Shaw DE, Mueller L, Prosser RS, Kobilka BK. Cell. 2013; 152:532–542. [PubMed: 23374348]
30. Orban T, Jastrzebska B, Gupta S, Wang B, Miyagi M, Chance MR, Palczewski K. Structure. 2012; 20:826–840. [PubMed: 22579250]
31. Kobilka BK. Trends. Pharmacol. Sci. 2011; 32:213–218. [PubMed: 21414670]
32. Koshland DE. Angew. Chem. Int. Ed. Engl. 1995; 33:2375–2378.
33. Imai H, Mizukami T, Imamoto Y, Shichida Y. Biochemistry. 1994; 33:14351–14358. [PubMed: 7947845]
34. Choe H-W, Park JH, Kim YJ, Ernst OP. Neuropharmacology. 2011; 60:52–57. [PubMed: 20708633]
35. Hofmann KP, Scheerer P, Hildebrand PW, Choe H-W, Park JH, Heck M, Ernst OP. Trends Biochem. Sci. 2009; 34:540–552. [PubMed: 19836958]
36. Dror RO, Arlow DH, Borhani DW, Jensen MO, Piana S, Shaw DE. Proc. Natl. Acad. Sci. USA. 2009; 106:4689–4694. [PubMed: 19258456]
37. Moukhametzianov R, Warne T, Edwards PC, Serrano-Vega MJ, Leslie AGW, Tate CG, Schertler GFX. Proc. Natl. Acad. Sci. USA. 2011; 108:8228–8232. [PubMed: 21540331]
38. Popovych N, Sun S, Ebright RH, Kalodimos CG. Nat. Struct. Mol. Biol. 2006; 13:831–838. [PubMed: 16906160]
39. Boehr DD, Nussinov R, Wright PE. Nat. Chem. Biol. 2009; 5:789–796. [PubMed: 19841628]
40. Liu W, Chun E, Thompson AA, Chubukov P, Xu F, Katritch V, Han GW, Roth CB, Heit-man LH, Ijzerman AP, Cherezov V, Stevens RC. Science. 2012; 337:232–236. [PubMed: 22798613]
41. Angel TE, Chance MR, Palczewski K. Proc. Natl. Acad. Sci. USA. 2009; 106:8555–8560. [PubMed: 19433801]
42. Angel TE, Gupta S, Jastrzebska B, Palczewski K, Chance MR. Proc. Natl. Acad. Sci. USA. 2009; 106:14367–14372. [PubMed: 19706523]
43. Seifert R, Wenzel-Seifert K, Gether U, Lam VT, Kobilka BK. Eur. J. Biochem. 1999; 260:661–666. [PubMed: 10102993]
44. Westfield GH, Rasmussen SGF, Su M, Dutta S, DeVree BT, Chung KY, Calinski D, Velez-Ruiz G, Oleskie AN, Pardon E, Chae PS, Liu T, Li S, Woods VL, Steyaert J, Kobilka BK, Sunahara RK, Skiniotis G. Proc. Natl. Acad. Sci. USA. 2011; 108:16086–16091. [PubMed: 21914848]

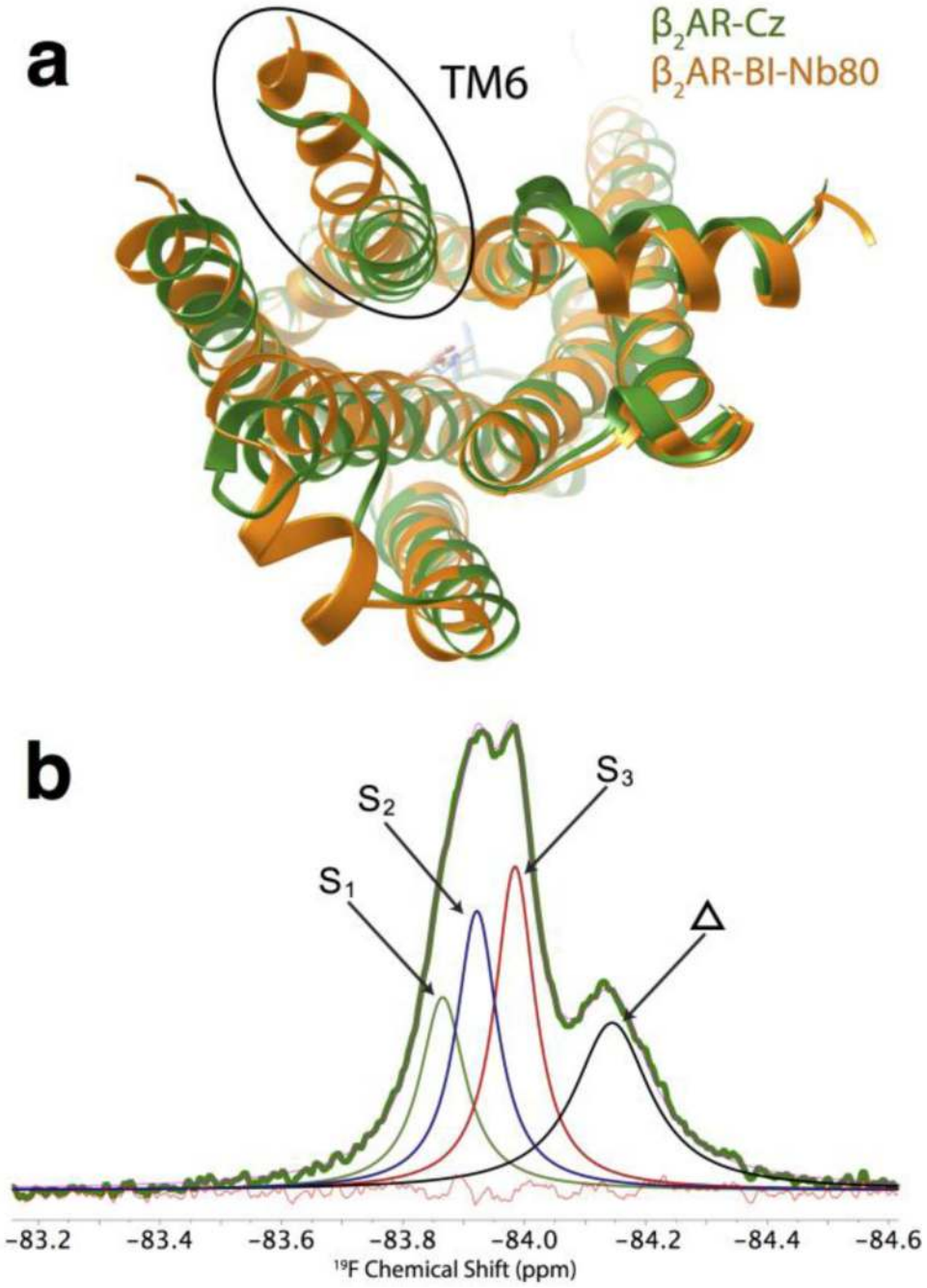

Figure 1.

(**a**) Superimposed crystal structures of Cz-bound β_2AR in green and BI-bound β_2AR with Nb80 in orange. The largest difference is at the end of TM6. (**b**) ^{19}F NMR spectrum of the apo form of β_2AR labeled with a trifluoromethyl tag at 30°C, showing a spectral deconvolution in which three distinct functional states of the receptor, S_1, S_2, and S_3, are identified. Note that this spectrum was published previously[20] but is shown here to introduce the states (S_1-S_3). An additional peak, Δ, designates a second partially labeled cysteine residue, which is not affected by ligands. The faint orange line designates the residual error associated with the fit.

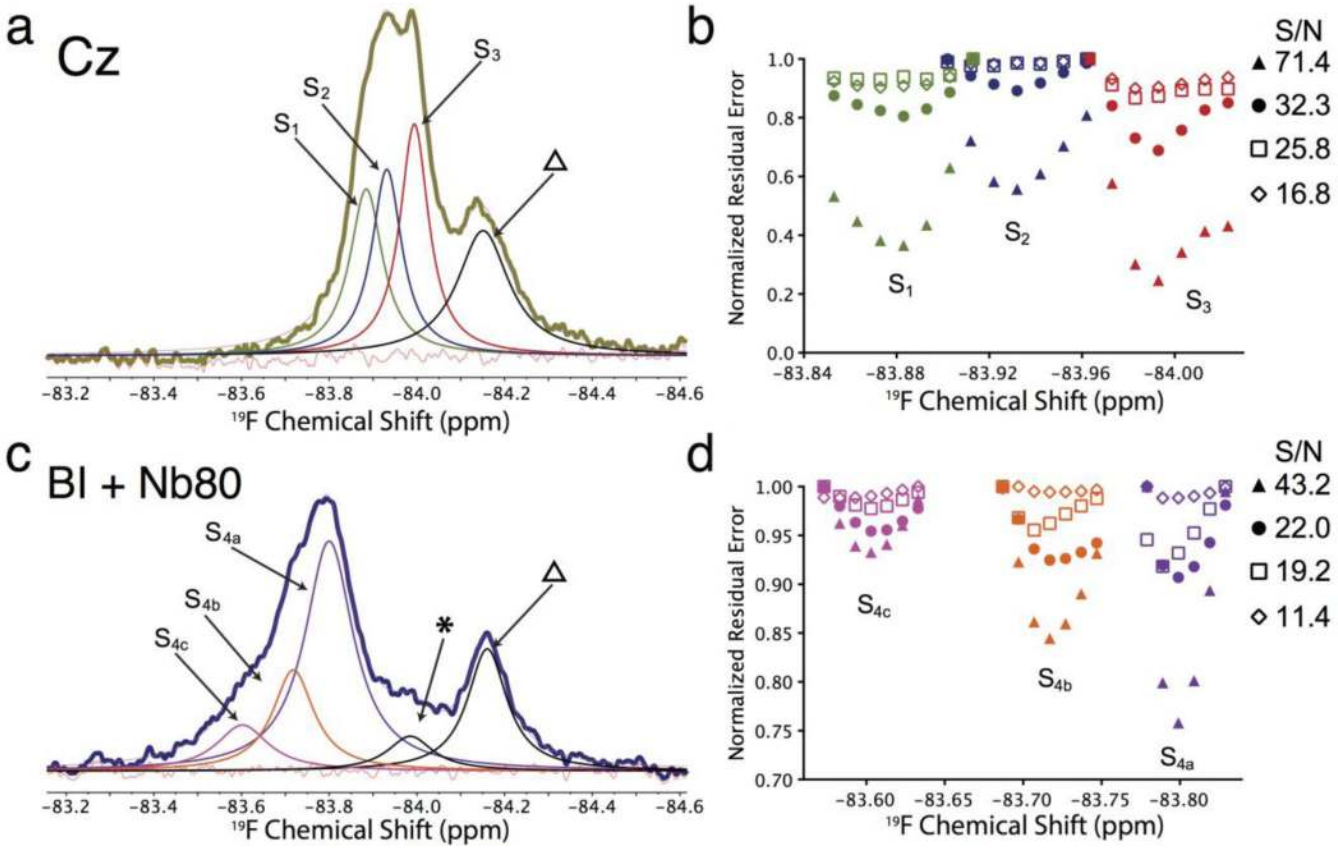

Figure 2.

Deconvolutions of ^{19}F NMR spectra of β_2AR, in the presence of saturating amounts of inverse agonist (**a**) or agonist plus Nb80 (**c**). Note that these spectra were published recently[20] but are recapitulated here to assess the robustness of the deconvolution fitting parameters. (**b**) An error analysis is performed where the effect of chemical shift offset on the global RMSD fitting error is separately explored for states, S_1, S_2, and S_3, defined by the deconvolution. The RMSD error is normalized by dividing the error resulting from a given offset, by that obtained for the greatest offset. An identical analysis is performed in (**d**) for the spectrum of β_2AR with nanobody. This error analysis is repeated in (b) and (d) as a function of overall signal to noise (S/N), resulting from the addition of noise to the spectra. The results show that with the given signal to noise ratio, states S_1, S_2, and S_3 can be robustly defined, while it is not possible to confidently ascribe three distinct conformers to the nanobody-stabilized spectrum.

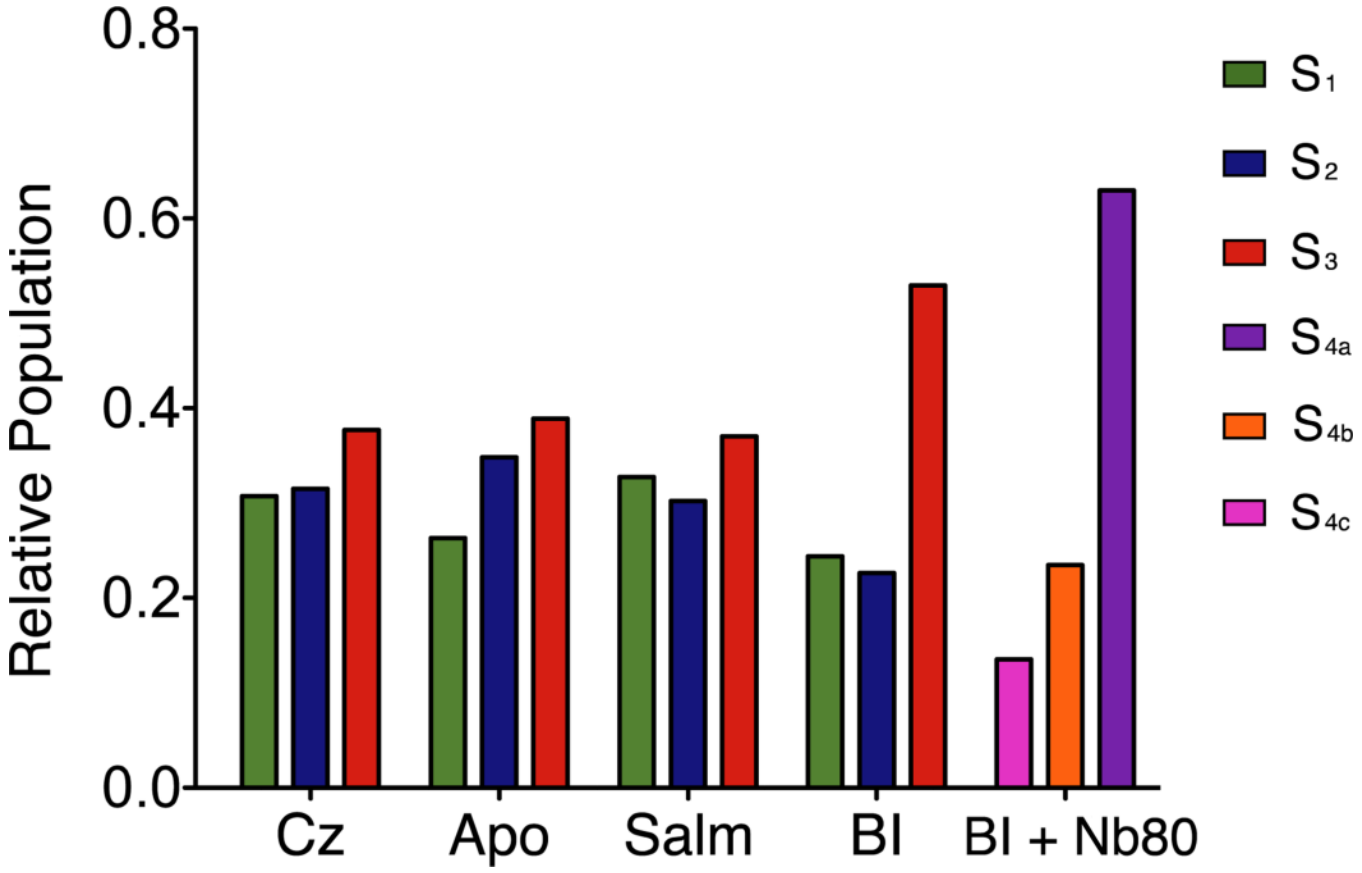

Figure 3.

Relative population of inactive (S_1 in green and S_2 in blue), activation intermediate (S_3 in red), and active states (S_{4a} in purple, S_{4b} in orange, and S_{4c} in magenta) as a function of ligand. Cz, Salm, and BI designate an inverse agonist (carazolol), a partial agonist (salmeterol), and a full agonist (BI-167107), respectively. Nb80 designates a nanobody, meant to mimic the stimulatory G protein, Gs.

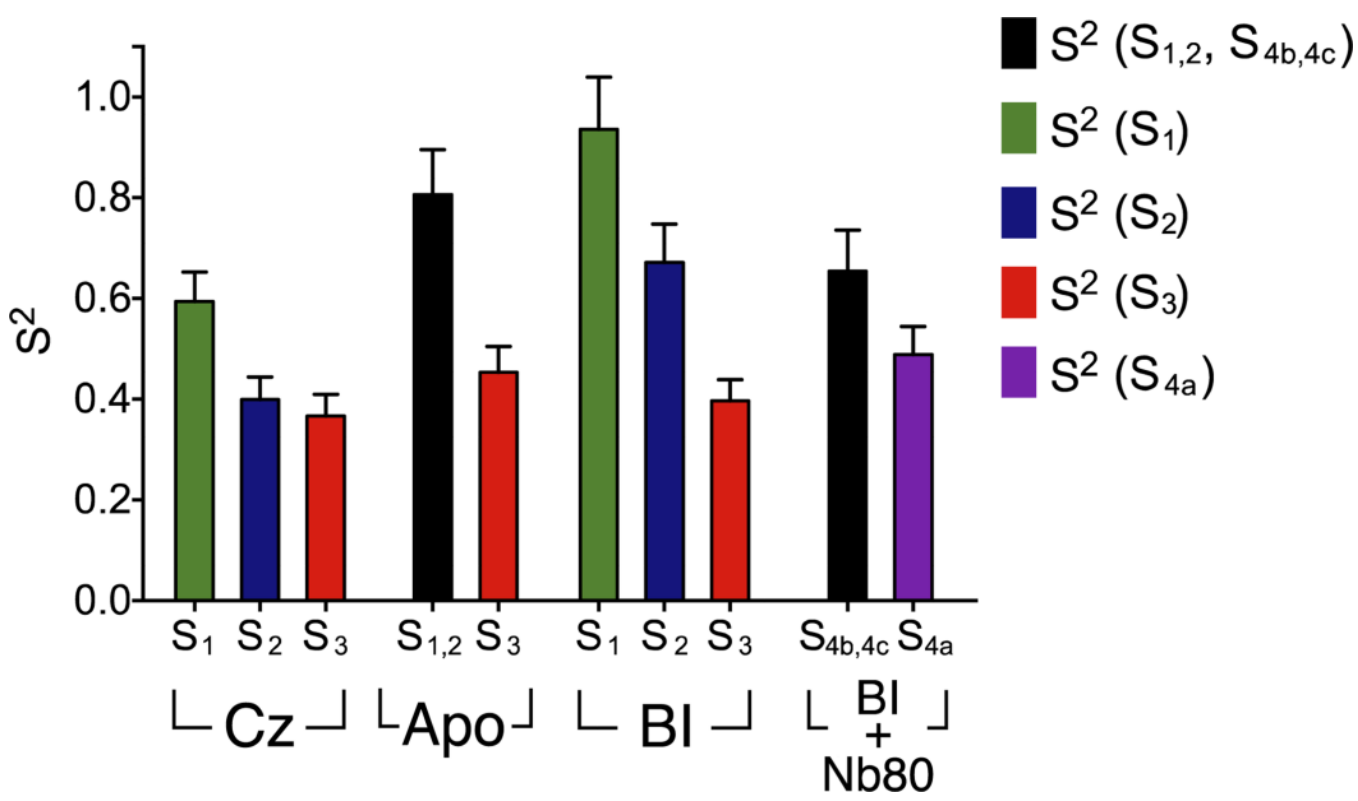

Figure 4.

Experimentally derived orientational order parameters, S^2 for the states, S_1, S_2, and S_3 in the apo state or in the presence of either inverse agonist (Cz) or agonist (BI). The orientational order of the active states, S_{4a}, S_{4b}, and S_{4c}, resulting from addition of Nb80 to the BI-saturated sample, are also included. Note that $S_{1,2}$ designates an average between states S_1 and S_2, which could not be reliably resolved in the order parameter analysis. Similarly $S_{4b,4c}$ represents an average of S_{4b} and S_{4c}.

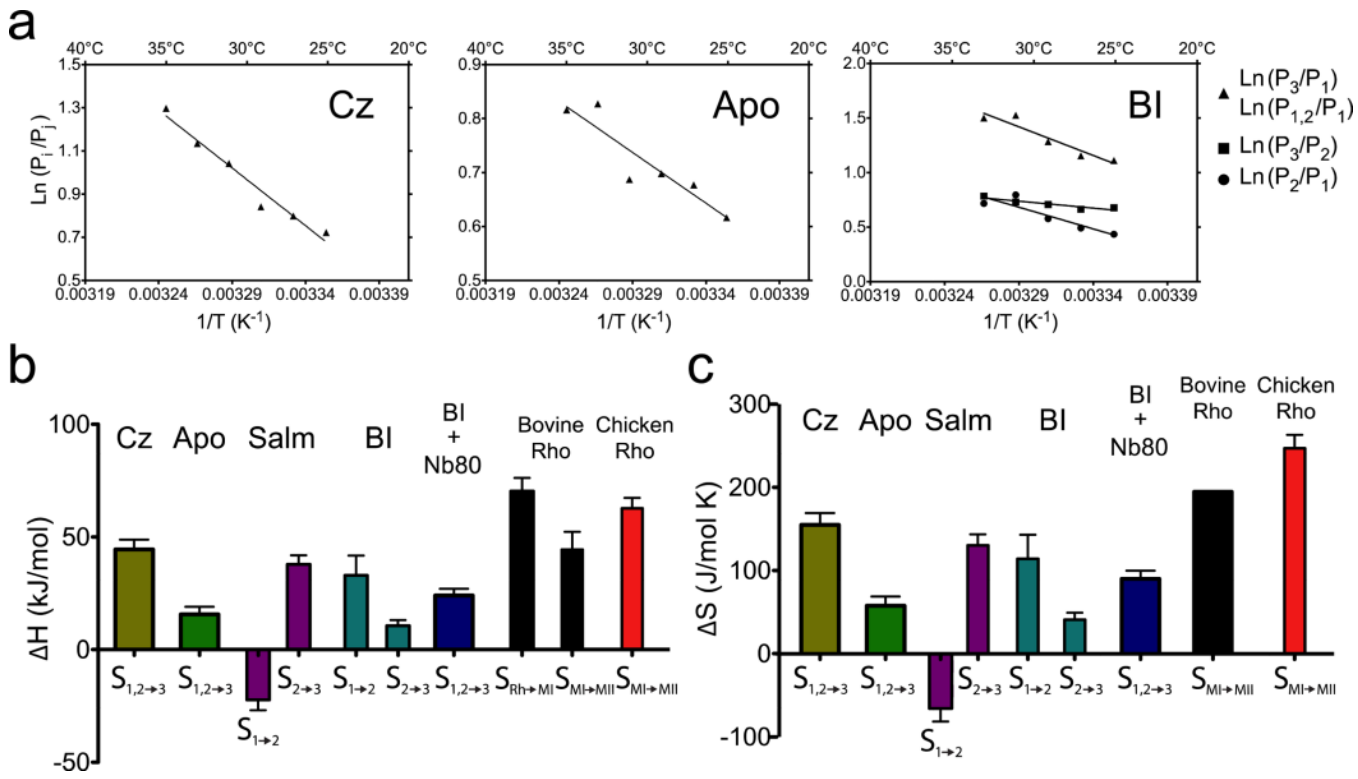

Figure 5.

(**a**) A van't Hoff analysis of the equilibrium constants, K_{31}, K_{32}, and K_{21} associated with β_2AR in the presence of the agonist, BI. (**b**), (**c**) Enthalpy (ΔH_{ij}) and entropy (ΔS_{ij}) differences between distinct functional states of β_2AR, as a function of ligand. Note that the corresponding enthalpy and entropy differences between inactive and active states of rhodopsin are provided for comparison.

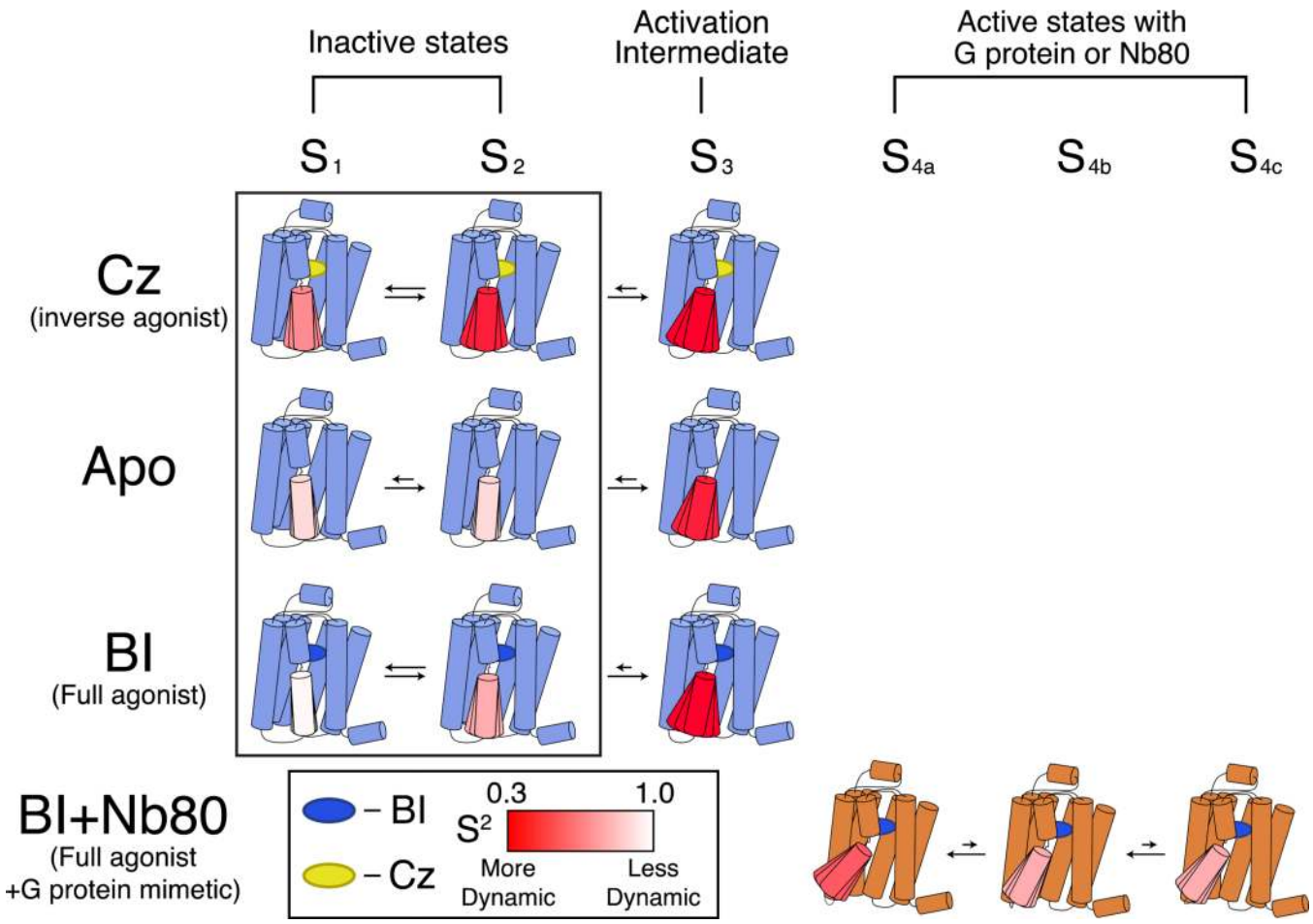

Figure 6.

A schematic illustrating the ensemble of states, identified by ^{19}F NMR and the effect of ligands and nanobody (Nb80) on both conformational equilibria and disorder of the cytosolic domain. For all ligands, there is an increasing trend in local dynamics of Cys265 with degree of activation while activation intermediate states (S_3) are the most dynamic among all states. In case of one of the inactive states, S_1, the local dynamics decrease as a function of efficacy of ligand. Note that active states are only accessible with a G protein or Nb80. Low order parameters (S^2) are represented in red while high order parameters being represented in white.